ANNALS of Faculty Engineering Hunedoara – International Journal of Engineering
Tome XX [2022] | Fascicule 4 [November]

[1.]Sunday O. ADETONA, [2.]Raifu I. SALAWU, [2]Najeem A. BELLO

MITIGATION OF TOTAL HARMONIC DISTORTION IN DOUBLE SPEED INDUCTION MOTOR USING LLCL BPF FOR INDUSTRIAL DRIVE SYSTEM

[1.]Department of Electrical & Electronics Engineering, University of Lagos, Lagos, NIGERIA
[2.]Department of Computer, Electrical & Electronics Engineering, The Bells University of Technology, Ota, NIGERIA

Abstract: The satisfactory performances of the 3-Ø induction motors (IMs) are greatly limited by the presence of harmonics. Many of the earlier works on alleviation of harmonics in IMs dwell much on single speed IMs (SSIM), despite the fact that they have limited applications. This research, therefore mitigate total harmonic distortion (THD) in double speed induction motor (DSIM) to achieve desire speed response in industrial drive system. A two-level, voltage source inverter (2L-VSI) was modeled and realized using Pulse Width Modulation (PWM) technique to power 15 kW 415 V DSIM. A LLCL band-pass filter (BPF) was substantiated for the 2L-VSI to filter the resulting THD separately on high and low speed. The proposed approach was implemented in MATLAB in the Simulink environment. The performance evaluations were carried out using harmonic of orders 5th to 13th for 2L-VSI without and with LLCL BPF with the DSIM. When the 2L-VSI was used to operate the DSIM without filter, the THD results relative to 5th and 7th order harmonics for the low and high speed operations of the DSIM were 66.23 % and 66.29 %, and 66.11% and 66.17 % respectively. When the 2L-VSI was used to operate the DSIM with the LLCL BPF, the THD results relative to 5th and 7th order harmonics for the low and high speed operations of the DSIM were 7.34 % and 7.41 % and 7.55 % and 7.62 % respectively. These results imply that the THDs are highly reduced to almost the same values for both speeds; and fall within the acceptable limit of the IEEE 519-2014.

Keywords: Passive filters, Double Speed Induction motor, Total Harmonic Distortion, Pulse Width Modulation, and Two Level Voltage Source Inverter

1. INTRODUCTION

Three phase induction motors (IMs) are extensively used motors in industrial applications due to self-starting, robust design, simple construction and high efficiency; but they are basically working at a constant speed [1][2]. Overtime, slip ring IMs are used for variable speed operations, but they have a complex design and high maintenance cost [3] compare to squirrel cage IMs. Today, squirrel cage IMs have taken over the operations of variable loads due to their ruggedness in harsh environments and friendly maintenance costs over slip ring IMs [4]; but they are mostly operated through variable frequency drives (VFD) to vary the speed of operation by changing the frequency or the voltage of the system to get the desired speed response easily [1] unlike the slip ring IMs that the speeds of control are usually done with the help of external resistance boxes connected to the slips of their rotors. But, the total harmonic distortion (THD) is still a subject of discussion in VFD for the operation of the squirrel cage IMs. The VFD is made up of power electronics converters; and as such, injected harmonics into the system. With the presence of harmonics, the sinusoidal voltage and current get disturbed; and fundamental frequency [5] gets deviated. This distortion if not handled correctly, can cause excessive heating, vibration, and humming among others, which will bring down the efficiency of the IM and eventually damage it [6].

For the purpose of addressing the negative consequences of harmonics distortions in the operation of IM that uses VFD, several pulse width modulation (PWM) techniques have been proposed like Selective harmonic elimination PWM (SHEPWM), Sinusoidal PWM (SPWM), Z-Source PWM, and Space vector modulation (SVM) [7][8]. Aside these methods, filters are also used for mitigation of harmonics generated through VFD and these are active, passive and hybrid filters depending on the configuration required for the eliminations of the THDs. For instance, the study in [9] addressed the issue of the mitigation of harmonics in adjustable speed drive using AC choke and C-type filters. The analysis was done without and with the proposed filters using a three-phase 2.3 kW, 1200 rpm IM; 0.95 modulation index Voltage Source Inverter (VSI) with SPMW; diode and IGBT as switching devices. Also, the work of [10] investigated the relationship between the modulation indexes of the modulated signal injected into a VSI fed 50 HP, 60 Hz IM against THD. The result obtained by [10] shows that the higher the modulation index, the lower the effect of the THD on the system. In order to make insignificant the THD in the line current of the IM, the study of [11] proposed the usage of combined optimal PWM waveforms. The study compared the results of the proposed combined PWM waveform with the SHEPWM waveform at the pulse number of 2 per quarter of the fundamental cycle on a 2.2 kW, 50 Hz IM drive. As good as the studies of above mentioned researchers; they are only centred on single speed IMs (SSIMs).

Meanwhile, as a result of tremendous changes in the application of IMs drive system, many industries like robotics, water cooperation, machine tools, and manufacturing companies have resulted in using double speed induction motor (DSIM) for most of their applications, where it is necessary to increase the output rate of their

productions. It is very clear that none of these researchers have carried out any research in this regard except only with SSIM; but the work of [12] examined operations and features of DSIM. In the work of [12], mechanical and electrical features of the machine were analysed under dissimilar functioning circumstances and at unlike rotating speeds. As good as the work of [12], the analysis of THD generated and methods that can be used in mitigating the THD were not discussed. As a result of this development, and in order to make a meaningful contribution to meet up with the new demand on IMs applications in industries, this study therefore, investigated the impact of THD levels in low and high speed of a DSIM; and also proposed utilization of LLCL BPF for reducing THDs in the DSIM fed through VFD

2. MATERIALS AND METHODS

— Dual Speed Induction Motor (DSIM)

The DSIM has two, $3-\emptyset$ stator windings separated apart, which share the same machine core and squirrel cage rotor winding. The stator windings are spatially shifted by an angle [13] and a rotor cage. The windings of the two stators can be supplied from a single (or different AC voltage sources, but of the same frequency with the help of external control circuit connection to avoid interactions between the two supplies) AC voltage source. Figure 1 presents the diagrammatic representation of the DSIM rotor and stator windings connections. The arrangement of parts of the DSIM resembles SSIM, except that its stator comprises of two windings that are displaced by an angle π/6 radians [12]. In Figure 1, α_1 and α_2 are the angles between the rotor phase r_a and the stator phases s_{a1} and s_{a2} respectively, θ is the offset angle between s_{a1} and s_{a2}. The circuits in Figure 2 represent the individual connection for the DSIM low and high speed configuration separately utilized. However, it requires an external control circuit connection for switching when motor is to be used at different times in the same operation.

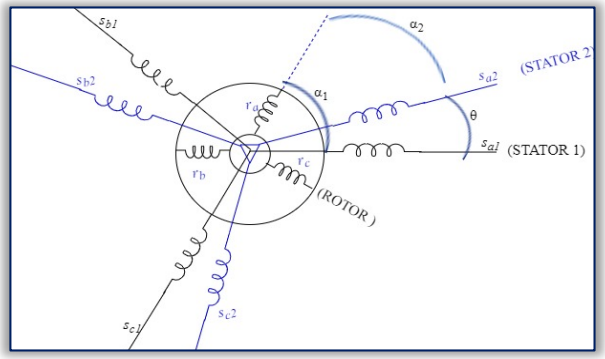

Figure 1. DSIM windings [12]

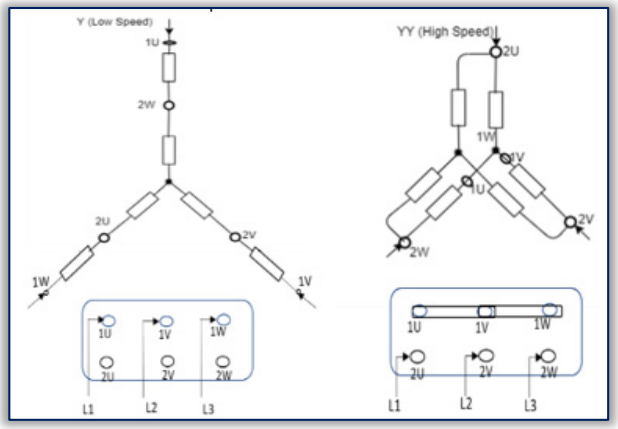

Figure 2. Internal and external connections of a DSIM [14]

— Mathematical Modeling of DSIM

Figure 3 presents an equivalent circuit of DSIM referred to the stator side. In the figure, R_{s1} and R_{s2} are s_{a1} and s_{a2} resistances respectively, $L_{s1}$and L_{s2} are s_{a1} and s_{a2} self-inductances respectively. The L_m is the cyclic mutual inductance between s_{a1}, s_{a2} and r_a. And, ω_s and ω_r are stator and rotor speeds in rad/s. $R_r{}' = R_r(\frac{N_s}{N_r})^2$, $L_r{}' = L_r(\frac{N_s}{N_r})^2$, $I_r{}' = (\frac{N_s}{N_r})I_r$; where, $R_r{}', L_r{}', I_r{}'$ are the rotor magnitudes referred to the stator.

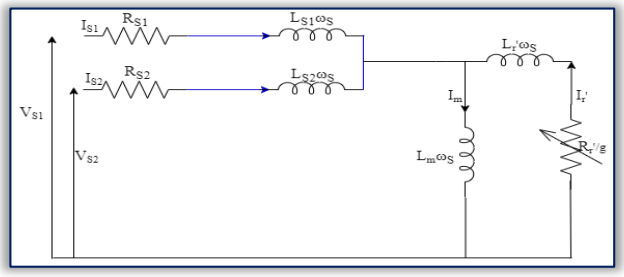

Figure 3. Equivalent circuit of DSIM referred to the stator side [12]

The equations of the s_{a1} and s_{a2} voltages, in the 2-phase reference of dq axis are

$$v_{ds1} = R_{s1}i_{ds1} + \frac{d\varphi_{ds1}}{dt} - \omega_s\varphi_{qs1} \quad (1)$$

$$v_{ds2} = R_{s2}i_{ds2} + \frac{d\varphi_{ds2}}{dt} - \omega_s\varphi_{qs2} \quad (2)$$

$$v_{qs1} = R_{s1}i_{qs1} + \frac{d\varphi_{qs1}}{dt} + \omega_s\varphi_{ds1} \quad (3)$$

$$v_{qs2} = R_{s2}i_{qs2} + \frac{d\varphi_{qs2}}{dt} + \omega_s\varphi_{ds2} \quad (4)$$

where, v_{ds1} and v_{ds2} are direct axis voltage for s_{a1} and s_{a2} respectively, v_{qs1} and v_{qs2} are quadrature axis voltage for s_{a1} and s_{a2} respectively. And the equations of the rotor voltages in the two-phase reference of dq axis are:

$$0 = R_ri_{dr} + \frac{d\varphi_{dr}}{dt} - \omega_{gl}\varphi_{qr} \quad (5)$$

$$0 = R_ri_{qr} + \frac{d\varphi_{qr}}{dt} + \omega_{gl}\varphi_{dr} \quad (6)$$

And with $\omega_{gl} = \omega_s - \omega_r$, the flux equations become

$$\varphi_{ds1} = L_{s1}i_{ds1} + L_m(i_{ds1} + i_{ds2} + i_{dr}) \quad (7)$$
$$\varphi_{ds2} = L_{s2}i_{ds2} + L_m(i_{ds1} + i_{ds2} + i_{dr}) \quad (8)$$
$$\varphi_{qs1} = L_{s1}i_{qs1} + L_m(i_{qs1} + i_{qs2} + i_{qr}) \quad (9)$$
$$\varphi_{qs2} = L_{s2}i_{qs2} + L_m(i_{qs1} + i_{qs2} + i_{qr}) \quad (10)$$
$$\varphi_{dr} = L_r i_{dr} + L_m(i_{ds1} + i_{ds2} + i_{dr}) \quad (11)$$
$$\varphi_{qr} = L_r i_{qr} + L_m(i_{qs1} + i_{qs2} + i_{qr}) \quad (12)$$

where, R_r is the rotor resistance, L_r is the rotor self-inductance; φ_{ds1} and φ_{ds2} are direct axis fluxes for s_{a1} and s_{a2} respectively; φ_{qs1} and φ_{qs2} are quadrature axis fluxes for s_{a1} and s_{a2} respectively; while, φ_{dr} and φ_{qr} are dq axis fluxes for the rotor. Also, i_{ds1} and i_{ds2} are direct axis currents for s_{a1} and s_{a2} respectively, i_{qs1} and i_{qs2} are quadrature axis currents for s_{a1} and s_{a2} respectively, while i_{dr} and i_{qr} are direct and quadrature axis currents for the rotor.

The torques generated by the s_{a1} and s_{a2} can be easily shown to be

$$T_{e1} = \frac{3}{2}p\frac{L_r}{L_m+L_r}(\varphi_{dr}i_{qs1} - \varphi_{qr}i_{ds1}) \quad (13)$$
$$T_{e2} = \frac{3}{2}p\frac{L_r}{L_m+L_r}(\varphi_{dr}i_{qs2} - \varphi_{qr}i_{ds2}) \quad (14)$$

where, p is the number of pole pairs; and knowing fully well that $T_e = T_{e1} + T_{e2}$; hence the torques generated by DSIM is

$$T_e = \frac{3}{2}P\frac{L_r}{L_m+L_r}[\varphi_{dr}(i_{qs1} + i_{qs2}) - \varphi_{qr}(i_{ds1} + i_{ds2}) \quad (15)$$

Eqs. (1) to (15) together with the DSIM parameters obtained from the field are used for the modelling of DSIM in the Simulink in the MATLAB environment. The DSIM employed in this study is a 15 kW, 415 V DSIM; and its specification is presented in Table 1. MATLAB 2019a, 64-bit version, was used in the realization of the Simulink model of the DSIM fed through VFD. A detailed specification of the 15 kW, 415 V DSIM used for this research was obtained from a name plate of an ABB motor operating as a pre-heater furnace recirculation fan motor for uniform distribution of heat in the furnace heating recirculation system.

Table 1. DSIM Specification

Characteristics	Value
Nominal power	15 kW
Line-to-line voltage	415 V
Frequency	50 Hz
Stator resistance	82.33 mΩ
Stator inductance	0.724 mH
Rotor resistance	50.3 mΩ
Rotor inductance	0.724 mH
Mutual inductance	27.11 mH
Inertia	0.37 kgm2
Friction factor	0.02791 Nms
Number of poles	4 for low-speed
	2 for high speed

— Two level Three-phase VSI as VFD

The synchronous speed $n\ (rpm)$ of an IM is a function of the frequency $f\ (Hz)$ and the number of poles p it possessed as related by

$$n = \frac{120f}{p} \quad (16)$$

Eq. (16) therefore reveals that when the frequency of the power supply is varied, the speed of the IM can be controlled to the required speed of operation; which can be achieved through the usage of VFD.

The schematic of the VFD employed in this research is presented in Figure 4; which reveals that it consists of the rectification and inverter units. The figure shows that a six-pulse bridge rectification unit was used as an input rectifier; and the peak voltage $(\hat{v}_{DC})$ of the rectification unit of the circuit is

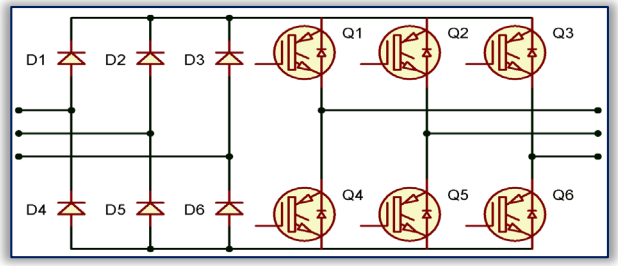

Figure 4. The circuit diagram of VFD

$$\hat{v}_{DC} = \sqrt{3}V_p = \sqrt{3}\sqrt{2}V_{rms} = \sqrt{6}V_{rms} \quad (17)$$

where, V_{rms} is 240 V; hence, $\hat{v}_{DC}$ is 587.8776 V.

In this study, the inverter stage involves the use of two-level $3-\emptyset$ voltage source inverter (2L-VSI) to control the speed of the $3-\emptyset$ DSIM. The power electronic switches used are insulated-gate bipolar transistors (IGBTs) which are turned on/off as required to produce varying voltage magnitude and frequency. Each leg of the inverter has two pairs of a combination consisting of an IGBT switch and a freewheeling diode while their middle point is linked to the DSIM. A freewheeling diode, connected in parallel, is required to conduct the current flow in the opposite direction to the IGBT; since IGBT can only conduct only in one direction. The six-step PWM was used to control the six IGBTs of the VSI. However, this approach has large harmonic components relative to the amplitude of the fundamental component of the output voltage. In order to account for harmonic currents and voltages in the DSIM fed VFD, we employed voltage and current Total Harmonic Distortion metrics; which are defined as

$$THD_I = \sqrt{\frac{\sum_{n\neq 1} I_n{}^2,\ rms}{I_1{}^2,\ rms}} = \frac{\sqrt{\sum_{n\neq 1,} I_n{}^2,\ rms}}{I_1{}^2,\ rms} \quad (18)$$

$$THD_V = \sqrt{\frac{\sum_{n\neq 1} V_n{}^2,\ rms}{V_1{}^2,\ rms}} = \frac{\sqrt{\sum_{n\neq 1,} V_n{}^2,\ rms}}{V_1{}^2,\ rms} \quad (19)$$

— Determination of switching frequency

The switching frequency f_s of any power electronic switching circuit, control signal frequency f_1, and frequency modulation ratio m_f are related by

$$m_f = \frac{f_s}{f_1} \quad (20)$$

Consequently, $f_s = f_1 m_f$, where $f_1 = 50\ Hz$; and, it has been established that the optimal value of m_f to give $\text{modulation index} \leq 1$ is 21 [15]. To that effect, $f_s = 50 \times 21 = 1050\ Hz$, and as such used in this study.

— The LLCL Band Pass Filter (BPF)

The VFD that normally employs PWM to control switching circuit of the VSI renders the required speed variations for the IM operations, increased IM reliability, and soft starting; but it generates large harmonics, which would reduce efficiency of IM, and give rise to excessive heat. In order to mitigate harmonic currents that may be flowing into DSIM, in this study, we employed and designed LLCL BPF [16]; and incorporated it in between VFD and DSIM. This is because the filter absolved resonance troubles, improves the system power factor, and maintains output voltage at no-load. The circuit diagram of the LLCL BPF is presented in Figure 5; which reveals that that the filter consists of small filter reactor L_0, shunt filter impedance L_f and C_f, and large filter reactor L_1; hence, named LLCL BPF.

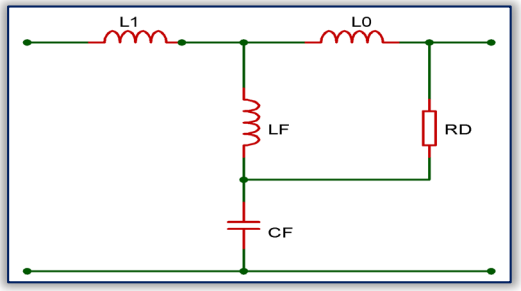

Figure 5. The LLCL BPF [16]

It has been suggested in [17] that IM should not be connected in series with an inductive element, therefore, a damping resistance R_d, was connected in parallel to the filter. At rife harmonics, the C_f and L_f of the filter render a low-impedance route to the dominant harmonics over a wide frequency range; whereas L_1 jams the flow of harmonic currents produced by the VFD into the DSIM, as well as, denigrates the upshot of line voltage harmonics on the DSIM.

— Design of LLCL BPF

It is straight forward to show that the parallel resonance (f_p) of the LLCL BPF is

$$f_p = \frac{1}{2\pi\sqrt{(L_1+L_f)C_f}} \quad (21)$$

In conformity with [16], the choice of f_p is a function of the fundamental frequency and the first dominant frequency of the harmonics generate by the circuit in question. In this study, a 6-pulse converters were used for the realization of the VFD, as such, its dominant harmonic orders k_d can be obtained using

$$k_d = 6k \pm 1 \quad (22)$$

Upon using Eq. (22), it is evident that the first k_d is 5; consequently, f_p is 250 Hz. If it is assumed that C_f, and L_f have the values of $3.5\ \mu F$ and 2.7 mH respectively; then L_1 will be

$$L_1 = \frac{1}{C_f}\left(\frac{1}{2\pi f_p}\right)^2 - L_f \approx 100\ mH \quad (23)$$

The value of the component L_0 according to [16] can be calculated by making use of

$$L_0 = \frac{0.04V^2}{\omega P_n} \quad (24)$$

where, P_n is the rated power of the DSIM, which is 15 kW; whereas, V is the line-to-line voltage; which is 415 volts in this study. Upon using the values of V, P_n and ω in Eq. (24), we obtained 1.462 mH for the value of L_0. And in accordance with [18], R_D is defined as

$$R_D = \frac{2\xi}{c_f\,\omega_{res}} \quad (25)$$

where, the resonance angular frequency $\omega_{res} = \sqrt{\frac{L_0+L_f}{L_0 L_f C_f}}$; and damping factor ξ is assumed to be 0.1 as recommended by [18]; then, the value of R_D used in this study is 3.3 Ω.

3. MODELLING AND SIMULATION

Figures 6 and 7 present Simulink models of the DSIM fed VFD without and with LLCL BPF respectively. The two models are implementable and executable in Simulink in the Matlab environment. Eqs. (1) through (15)

together with the DSIM parameters obtained from the field are used for the modelling the block of DSIM fed 2L-VSI in the Simulink in the MATLAB 2019a environment; whereas, the VFD model is realized by using information deducible in Eqs. (16) through(20), and the model of LLCL BPF is achieved by making used of parameters obtained in Eqs. (20) to (25).

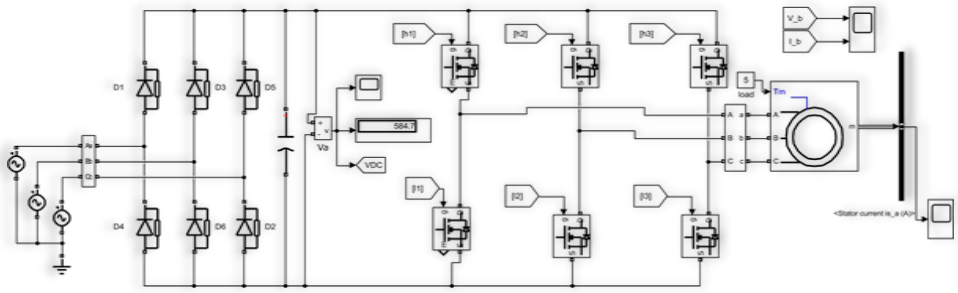

Figure 6. Simulink model of the DSIM fed by 2L-VSI without LLCL BPF

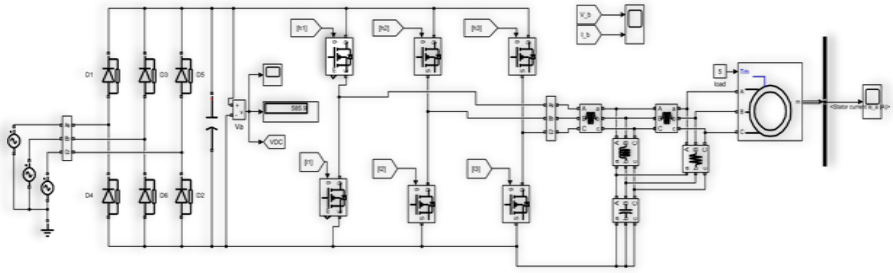

Figure 7. Simulink model of the DSIM fed by 2L-VSI with LLCL BPF

4. RESULTS AND DISCUSSION

— Simulation Analysis of THD in DSIM

This subsection presents the results of the THD obtained from operations of the 15 kW DSIM in low and high speeds configurations connected to the VSI in the Simulink in the Matlab environment using FFT tool. Figures 8 and 9 show the simulation results of both conditions. The THD results relative to 5th order harmonics for the low and high speeds are 66.23 % and 66.11 %, respectively; whereas, for the 7th order harmonics for the low and high speeds are 66.29 % and 66.17 %, respectively.

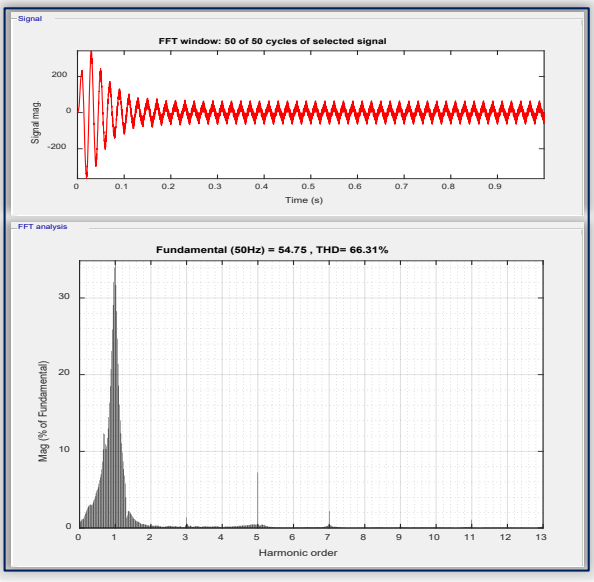

Figure 8. THD without filter for 15 kW DSIM in low speed configuration

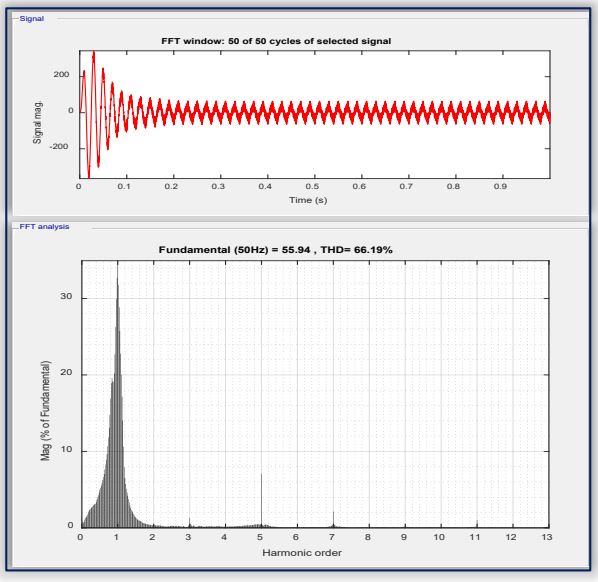

Figure 9. THD without filter for 15 kW DSIM in high speed configuration

— Total Harmonic Distortion Mitigation

In order to mitigate the THD in the stator of DSIM, a LLCL BPF was designed and connected in between DSIM and VFD. The results of the THD obtained when the DSIM is operated with VSI without insertion of the LLCL BPF give high percentage values which can cause damage to the DSIM due to excessive heating, vibration and humming. This requires reduction in order to avert the possible problems. In this part, reduction of THD is carried out with the insertion of the designed filter; and the current measured at the point of common coupling

with the DSIM without short-circuit fault and in the presence of the fault. This is necessary in order to determine the THD set limit for the DSIM according to IEEE 519-2014[19] standard.

The maximum load current $\mathbf{I_L}$ is obtained by connecting the DSIM directly to the output of the 2L-VSI; while the three phase output of the 2L-VSI is shorted after disconnecting the DSIM to get the maximum short-circuit current $\mathbf{I_{sc}}$. At the PCC, $\mathbf{I_L}$ is 25.34A while $\mathbf{I_{sc}}$ is 3311A; as such, the ratio $\mathbf{I_{sc}/I_L = 130.66}$. According to IEEE 519-2014 [19], the maximum allowable THD for $\mathbf{100 < I_{sc}/I_L < 1{,}000}$ and current distortion limits for systems rated 120 V through 69 kV is 15 %. The voltage level of line-to-line used for this model is 415 V; hence, the THD must be reduced to a maximum of 15 %.

— THD Mitigation with LLCL BPF for Low and High Speeds

The stator current with the use of LLCL BPF and the corresponding THD relative to 5th and 7th harmonics at low and high speeds are shown in Figures 10 and 11 respectively.

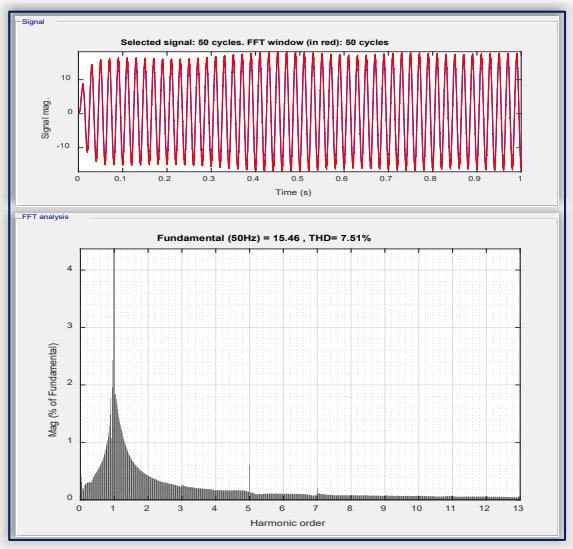

Figure 10. THD for low-speed DSIM using LLCL BPF

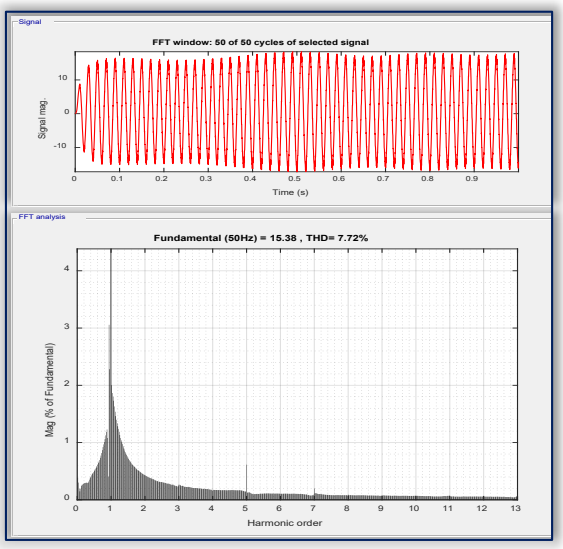

Figure 11. THD for high-speed DSIM using LLCL BPF

It can be seen that the THD relative to 5th and 7th harmonic orders were reduced from 66.23 % and 66.29 % without the filter to 7.34 % and 7.41 % respectively when the LLCL BPF is applied for low speed operation; and 7.55 % and 7.62 % for high speed respectively at the point of connecting the DSIM to the VSI.

5. DISCUSSION

The summary of the results obtained from the simulation of DSIM is shown in Table 2 and the outcomes are compared to show the most effective THD reduction of the DSIM.

Table 2. Summary of the results obtained from the simulation of DSIM

Configuration	Low Speed				High Speed			
Order (%)	5th	7th	11th	13th	5th	7th	11th	13th
2L-VSI without BPF	66.2	66.3	66.3	66.3	66.1	66.2	66.2	66.2
2L-VSI with BPF	7.34	7.41	7.49	7.51	7.55	7.62	7.7	7.72

When the 2L-VSI is used to operate the DSIM without filter, the THD results relative to 5th and 7th order harmonics for the low and high speed operations of the DSIM are 66.23 % and 66.29 %, and 66.11% and 66.17 % respectively. These show that the THDs are relatively high and the same for low and high speed operations of the DSIM when 2L-VSI are utilised without filter. Furthermore, injection of LLCL BPF to the 2L-VSI reduces the THDs relatively to 5th and 7th harmonics to 7.34 % and 7.41 % and 7.55 % and 7.62 %, respectively for low and high speed operations of DSIM. These imply that the THDs are highly reduced to almost the same values for both speeds. The results fall within the acceptable limit of the IEEE 519-2014 standard of 15 %.

6. CONCLUSION

This study investigated the upshot of THD levels in low and high speed of a DSIM; and also proposed utilization of LLCL BPF for reducing THDs in the DSIM fed through VFD. The proposed approach was implemented in MATLAB in the Simulink environment. A 2L-VSI was modeled and realized using PWM technique to power 15 kW 415 V DSIM. A LLCL BPF was substantiated for the 2L-VSI to filter the resulting THDs separately on high and low speed. The performance evaluations were carried out using harmonic of orders 5th to 13th for 2L-VSI without and with LLCL BPF with the DSIM. Analysis were done to see which of the conditions conformed with IEEE standard 519-2014 of 15 % for IM rating in this category both for high and low speed operations. The simulation results show that the THDs of the low and high speed of the DSIM are relatively equal and hugely reduced when 2L-VSI with LLCL BPF is used.

Nomenclature

r_a	Rotor phase
s_{a1}	Stator 1 phase
s_{a2}	Stator 2 phase
α_1	Angles between r_a and s_{a1}
α_2	Angles between r_a and s_{a1}
θ	The offset angle between s_{a1} and s_{a2}
R_r	The r_a resistance
R_{s1}	The s_{a1} resistance
R_{s2}	The s_{a2} resistance
L_r	The r_a self-inductance
L_{s1}	The s_{a1} self-inductance
L_{s2}	The s_{a2} self-inductance
L_m	Mutual inductance between s_{a1}, s_{a2} and r_a
ω_s	Stator speed in rad/s,
ω_r	Rotor speed in rad/s
R_r', L_r', I_r'	The R_r, L_r and I_r referred to the stator
d, q axis	Direct and quadrature axis
v_{ds1}	Direct axis voltage for s_{a1}
v_{ds2}	Direct axis voltage for s_{a2}
v_{qs1}	Quadrature axis voltage for s_{a1}
v_{qs2}	Quadrature axis voltage for s_{a1}
φ_{ds1}	Direct axis flux for s_{a1}
φ_{ds2}	Direct axis flux for s_{a2}
φ_{qs1}	Quadrature axis flux for s_{a1},
φ_{qs2}	Quadrature axis flux for s_{a2}
φ_{dr}	Direct axis flux for r_a
φ_{qr}	Quadrature axis flux for r_a
i_{ds1}	Direct axis currents for s_{a1}
i_{ds2}	Direct axis currents for s_{a2}
i_{qs1}	Quadrature axis currents for s_{a1}
i_{qs2}	Quadrature axis currents for s_{a2}
i_{dr}	Direct axis current for r_a
i_{qr}	Quadrature axis current for r_a
T_{e1}	Torque generated by the s_{a1}
T_{e2}	Torque generated by the s_{a2}
p	Number of pole pairs
n (rpm)	Synchronous speed of an IM
f (Hz)	Frequency
$\hat{v}_{DC}$	Peak voltage of the rectifier of the VFD
f_s	Switching frequency
f_1	Control signal frequency,
m_f	Frequency modulation index
L_0	Small filter reactor of the LLCL BPF
L_f and C_f	Shunt filter impedance of the LLCL BPF
L_1	Large filter reactor of the LLCL BPF
f_p	Parallel resonance of the LLCL BPF
ω_{res}	Resonance angular frequency
P_n	The rated power of the DSIM
V	The line-to-line voltage
R_d	Damping resistance
ξ	Damping factor
I_L	Maximum load current
I_{sc}	Short–circuit current

Acknowledgment

The authors are pleased to acknowledge the support provided by the Department of Electrical, Electronics and Computer Engineering, Bells University of Technology, Ota, Ogun State, Nigeria.

References

[1] Abhishek, C., and Vinay, P.: Analysis of harmonics of PWM controlled induction motor using Fast Fourier Transform tool. Advanced Research in Electrical and Electronic Engineering, 2(6), 4-6, 2015.

[2] Reddy, S. K., Ramachandran, A., Muralidhara V., and Srinivasan R.: Simulation with Experimental Measurement of Voltage Total Harmonic Distortion and Harmonic Frequency in Three-Phase Induction Motor fed from Inverter. Proceedings of the World Congress on Engineering, (1), 5-7, 2017.

[3] Vinod N. M., Kalpesh J. C., and Yogesh M. M.,: Three Phase Slip Ring Induction Motor Drive with Slip Power Control Analysis for Different Load Torque using Microsoft Excel as Software tool. Proceedings of the 2008 International Conference on Modeling, Simulation & Visualization Methods, 270-275, 2008.

[4] Shukla N.K., and Srivastava R.: Performance evaluation of three phase induction motor using MOSFET & IGBT based voltage source inverter. International Research Journal of Engineering and Technology, 4(6), 2026-2031, 2017.

[5] Cheepati, K.R., and Prasad, T.N.: Importance of passive harmonic filters over active harmonic filters in power quality improvement under constant loading conditions. IOSR Journal of Electrical and Electronics Engineering, 21-27, 2016.

[6] Mohitkar, S.S., and Dhend, M.H.: Harmonic measurement and analysis of variable frequency drive in industry. International Journal of Research in Advent Technology, 2(2), 303-309, 2014.

[7] Shen, M., and Peng, F.Z.: Operation modes and characteristics of the Z-source inverter with small inductance or low power factor. IEEE transactions on industrial electronics, 55(1), 89-96, 2008.

[8] Shen, M., Wang, J., Joseph, A., Peng, F.Z., Tolbert, L.M., and Adams, D.J.: Constant boost control of the Z-source inverter to minimize current ripple and voltage stress. IEEE transactions on industry applications, 42(3), 770-778, 2006 .

[9] Uma, D., Vijayarekha, K., and Anupama, V.R.: Mitigation of harmonics and inter-harmonics in adjustable speed drives. International Journal of Engineering and Technology, 5(3), 2790- 2799, 2013.

[10] Neha, I.T., and Rakesh, S.L.: THD analysis of output voltage for VSI fed induction motor drives. International Journal of Engineering and Management Research, 4(4), 130-133, 2014.

[11] Rai, N., Rai, B., and Maheshwari, A.: Evaluation and minimization of total harmonic distortion in two level voltage-source inverter fed induction motor drives. International Conference on Current Trends towards Converging Technologies, 1-7, 2013.

[12] Oumar, A., Chakib, R., and Cherkaoui, M.: Performance and characteristics of double star induction machine. International Conference on Systems and Control, 399-404, 2019.

[13] Pienkowski, K..: Analysis and control of dual stator winding induction motor. Institute of Electrical Machines, Drives and Measurements Wroclaw University of Technology Wybrzeże Wyspiańskiego 27, 50-370 Wroclaw, Poland, 61(3), 421-438, 2012.

[14] Cantoni Motor, (2009). Catalogue. Retrieved from https://pdf.directindustry.com/pdf/cantoni-motor/multi-speed-three-phase-induction-motors/32165-588811.html. Accessed 12th March, 2020.
[15] Askar, M.E., and Kilic, H.: Modulation index and switching frequency effect on symmetric regular sampled SPWM. European Journal of Technic., 7(2), 102-109, 2017.
[16] Das, J.C.: Power system harmonics and passive filter designs. New Jersey: John Wiley and sons, 704-706, 2015.
[17] MATLAB 2018a: The MathWorks, Inc., Natick, Massachusetts, United States.
[18] Kahlane, A.W., Hassaine, N., and Kherchi, M.: LCL filter design for voltaic grid connected systems. Revue des Energies Renouvelables SIENR'14 Ghardala, 227-232, 2015.
[19] IEEE Power and Energy Society: IEEE Recommended Practice and Requirements for Harmonic Control in Electric Power Systems. New York: IEEE, 2014.


ISSN 1584 – 2665 (printed version); ISSN 2601 – 2332 (online); ISSN-L 1584 – 2665